Thin Solid Films 544 (2013) 324–330

Contents lists available at ScienceDirect

Thin Solid Films

journal homepage: www.elsevier.com/locate/tsf

Properties of magnetron-sputtered moisture barrier layer on transparent polyimide/graphene nanocomposite film

Mei-Hui Tsai [a], Chi-Jung Chang [b], Horng-Hwa Lu [c], Yu-Fu Liao [a], I-Hsiang Tseng [b,*]

[a] Department of Chemical and Materials Engineering, National Chin-Yi University of Technology, No. 57, Sec. 2, Chungshan Rd., Taipin Dist., Taichung, 41170, Taiwan
[b] Department of Chemical Engineering, Feng Chia University, No. 100, Wenhwa Rd., Seatwen Dist., Taichung, 40724, Taiwan
[c] Department of Mechanical Engineering, National Chin-Yi University of Technology, No. 57, Sec. 2, Chungshan Rd., Taipin Dist., Taichung, 41170, Taiwan

ARTICLE INFO

Available online 6 March 2013

Keywords:
Transparent polyimide
Graphene
Water-vapor-transmission-rate
Silicon nitride
RF magnetron sputtering

ABSTRACT

Colorless polyimides (PIs) have been considered as potential substrates for flexible displays due to their excellent transparency, thermal stability, mechanical strength and flexibility. However, high water vapor transmission rate (WVTR) of PI films limits the lifetime of electronic devices using PI films as substrates. Two approaches were applied to reduce the WVTR of PI films. Graphene (RG), which is thermally reduced graphene oxide (GO), was blended with a nearly colorless PI solution synthesized from an alicyclic tetracarboxylic dianhydride and aromatic diamine in cosolvent to obtain PI/RG nanocomposites. Subsequently, a barrier thin film was deposited on those PI nanocomposites by radio frequency magnetron sputtering from a Si_3N_4 target. The deposited barrier layer was amorphous and its composition along the thickness was homogeneous based on the X-ray diffraction patterns and the depth profile by X-ray photoelectron spectroscopy. An optimum deposition thickness of the barrier layer is 30 nm to obtain a close-packed, smooth and continuous barrier film on PI. The presence of a 30 nm-thick barrier layer on PI/RG-0.1 nanocomposite film capably reduces the WVTR to 0.17 g/m^2-day compared to 181 g/m^2-day for pure PI and 13 g/m^2-day for PI/RG-0.1. The surface of PI/RG is more hydrophobic and the capacity of moisture absorption by PI/RG is lower than PI/GO indicating the water resistance by RG is superior to that by GO. This flexible nanocomposite film remains high optical clarity and simultaneously shows excellent water barrier performance, enhanced dimensional stability and sufficient mechanical strength for advanced electronic applications.

1. Introduction

Polyimides (PIs) are considered as promising materials for flexible displays due to their flexibility, light weight and robust [1–5]. However, the orange-yellow color of traditional aromatic PIs limits their applications and the high water vapor transmission rate (WVTR) reduces the lifetime of electronic devices using PIs as flexible substrates [1,3,5]. Hence, several approaches have been made to develop transparent polymer substrates with improved barrier property [6,7]. The water or gas permeability of polymers can be reduced by atomic layer deposition or chemical vapor deposition of inorganic materials, such as Al_2O_3, SiO_2 and SiN_x, on polymer substrates [5,8–10]. The WVTR of the Langmuir–Blodgett-coated Kapton film (thickness: 75 μm) drops from 168 g/m^2-day to as low as 28 g/m^2-day [11]. The PI films with relatively rigid structure exhibit lower WVTR [12]. In addition, the relatively rigid PI matrix leads to a denser packing of a barrier layer on PI, and thus rigid PI exhibits lower moisture permeability than flexible PI [13,14].

Recently, the graphene-related nanofillers have been considered as promising gas barrier materials [15,16] for polymer matrix. An improved barrier property of transparent PI by blending with graphene oxide (GO) was observed from our preliminary result [17]. The matrix of transparent PI is not as rigid as that the WVTR of transparent PI is higher than traditional PI. Hence, an improved barrier property is essential before those transparent PIs applied to electronic industry. Two approaches were applied to reduce the WVTR of transparent PI films in this study. Transparent PI solution was blended with small amount of graphene (RG) to synthesize PI/RG nanocomposite films in order to reduce its WVTR and simultaneously retain its transparency. Subsequently, a barrier layer was deposited on PI/RG nanocomposite films by a radio frequency (RF) magnetron sputtering process to further reduce the water permeation. A silicon nitride (Si_3N_4) target was selected to deposit a single barrier layer on PI/RG nanocomposite film because it is transparent and has been considered as a superior moisture resistance material for semiconductor applications [8,18]. The deposition parameters were optimized to obtain the best barrier property, i.e. the lowest WVTR value, of flexible and transparent PI/RG nanocomposite films. The composition and morphology of deposited barrier layer as well as the optical, thermal and mechanical properties of PI/RG nanocomposites were comprehensively investigated in this work.

* Corresponding author. Tel.: +886 4 24517250x3666; fax: +886 4 24510890.
E-mail address: ihtseng@fcu.edu.tw (I.-H. Tseng).

0040-6090/$ – see front matter © 2013 Elsevier B.V. All rights reserved.
http://dx.doi.org/10.1016/j.tsf.2013.02.105

2. Experimental details

2.1. Materials

Bicyclo[2.2.2]oct-7-ene-2,3,5,6-tetracarboxylic dianhydride (BCDA) and 3,4′-oxydianiline (3,4′-ODA) purchased from Aldrich were used as-received. The solvents γ-butyrolactone (GBL) and dimethylacetamide (DMAc) were provided by TEDIA. The catalyst isoquinoline for preparing PI and chemicals HCl, H_2SO_4, H_2O_2 and $KMnO_4$ for synthesizing GO or RG were commercially obtained from TCI. Graphite powder (325 mesh) was supplied by Alfa-Aesar.

2.2. Synthesis of PI solution

Organo-soluble PI with solid content of 20 wt.% was synthesized from the reaction of equal molar BCDA and 3,4′-ODA in cosolvent via one-step method. A typical batch containing 3,4′-ODA (3.5526 g) and BCDA (4.4474 g) was completely dissolved in the co-solvent (GBL and DMAc, 16 g) and continuously mixed by a mechanical stirrer at room temperature under N_2. After 2 h, the isoquinoline was mixed with the above solution and continuously refluxed at 170–180 °C for 18 h to complete the imidization process. The resultant viscous and transparent PI solution was cooled and slowly decanted into excess methanol to solidify PI. The PI precipitate was continuously stirred in methanol to remove unreacted monomers or low-molecular-weight PI segments. After drying in a vacuum oven at 150 °C, the collected PI precipitate can be stored or easily re-dissolved in DMAc for casting pure PI films or preparing PI/GO or PI/RG nanocomposites.

2.3. Preparation of GO and RG nanosheets

A modified Hummers method [17,19,20] was utilized to synthesize GO nanosheets. The natural graphite (3 g) was mixed with $NaNO_3$ (3 g) and concentrated H_2SO_4 (50 mL) in a 250 mL three-neck flask in an ice bath, and followed by the slow addition of 15 g of $KMnO_4$. The mixture was continuously stirred for 48 h and then H_2O_2 (35 mL) was slowly added into the mixture. The fully oxidized suspension was poured into a large amount of distilled water. The solid products were obtained after the washing process with 10% HCl solution to achieve a pH value of 6. The precursor was dried at 60 °C in a vacuum oven for one night to obtain GO. GO powders were calcinated in a furnace at a heating rate of 2 °C/min, from room temperature to 1050 °C, isothermal for 10 min, under Ar to obtain RG powder.

2.4. Preparation of PI/GO and PI/RG nanocomposites

The dried PI precipitate (1.5 g) was completely dissolved in DMAc to obtain PI solution with the solid content of 20 wt.% at ambient condition. For preparing PI containing 0.1 wt.% of RG, RG (0.0015 g) suspended in DMAc (2 g) was ultrasonicated for at least 2 h and then mixed with the above PI solution at room temperature. The degassed PI/RG solution was cast on a clean glass substrate by a doctor-blade. A reference pure PI sample was also cast by using the pure PI solution. All the cast films were under heat treatment at a rate of 0.5 °C/min to 100, 140, 160 and 180 °C, isothermal at each temperature for 1 h, and finally to 210 °C for 5 h to completely remove the solvents. The sample code is denoted PI/RG-x, where x indicates the weight percentage of RG in final hybrid film. The reference PI/GO samples denoted PI/GO-y were also prepared via the same procedure except blending certain amount of GO (y wt.%) in PI solution.

2.5. Deposition of barrier film on PI films

The barrier film was deposited on pure PI or PI nanocomposite films by a RF magnetron sputtering system using a Si_3N_4 target under Ar. The sputtering parameters including power (50, 80 or 100 W) and working pressure (4, 6 or 8 mTorr) were adjusted to deposit barrier film with the thickness ranging from 20 to 100 nm on the surface of PI films. The barrier layer-deposited PI films were denoted Si-z/PI, Si-z/PI/RG-x or Si-z/PI/GO-y, respectively, indicating the thickness (z, in the unit of nm) of deposited film on pure PI, PI/RG-x or PI/GO-y nanocomposite films.

2.6. Characterization

The crystalline structures of GO, RG and deposited films were identified by X-ray diffraction (XRD) using a Shimadzu XRD-6000 equipped with a CuKα radiation ($\lambda = 0.154$ nm) at 40 kV and 30 mA. An X-ray photoelectron spectrometer (XPS) (ESCA PHI-1600, Physical Electronics) was used to determine the surface composition of nanofillers and the deposited film. The XPS depth profile was performed by using an Ar^+ ion gun at a sputtering rate of 14.3 nm/min on the barrier layer. The field emission scanning electron microscope (FE-SEM, JEOL JSM-7401F) was performed at an acceleration voltage of 15 kV to observe the morphology of the fractured surface of PI/RG film and the surface of deposited thin film. The atomic force microscope (AFM, Veeco, D5000) was also utilized to analyze the surface roughness of deposited barrier layer. The transmission electron microscope (TEM, JEOL JEM-2100F) equipped with EDS (OXFORD, X-MAX) was applied at an acceleration voltage of 200 kV to observe the morphology of RG. The UV–vis spectra of PI nanocomposite films were examined by a UV–vis/color spectrophotometer (HUNTERLAB, Ultrascan VIS). The WVTR of each sample with the size of 10 cm^2 was measured using a permeation test system (MOCON, Permatran-W 3/61) at atmospheric pressure, 40 °C and 100% relative humidity (RH). The WVTR (g/m^2-day) of each sample multiplied by film thickness (1 mil = 25 μm) is the water vapor permeation with the unit of g-mil/m^2-day. The dynamic mechanical analysis (DMA) was performed with a Dupont DMA-2980 at a frequency of 1 Hz, from 60 to 400 °C and at a heating rate of 3 °C/min. Thermogravimetric analysis (TGA) was carried out with a TGA-Q500 from TA Instrument at a heating rate of 20 °C/min under nitrogen. The thermal mechanical analyzer (TMA, TA Instrument, Q-400) was conducted under an extension mode, with a tension force of 0.05 N, at a heating rate of 10 °C/min, at a frequency of 1 Hz and under nitrogen. The coefficient of thermal expansion (CTE) was determined by the dimension change in the temperature range of 100 to 200 °C, which is the commonly applied testing condition in manufacturers.

3. Results and discussion

3.1. Characteristics of GO and RG

The surface composition of RG was examined by the analysis of its XPS spectra. Fig. 1(a) illustrates the raw data and deconvoluted results in C1s region of RG. The graphitic C═C and C – C structures were revealed at the binding energy of 284.2 and 284.7 eV, respectively [21–23]. Compared with previous XPS results of GO [17,24], the intensity of graphitic C═C components on RG increased indicating the slight restoration process during the thermal reduction of GO. In addition, the intense splitting of the C1s peak at higher binding energy was negligible suggesting fewer oxidized carbon functional groups, including C – OH (286.5 eV) and C – O – C (286.8 eV), remained on RG [21,23,25] after the thermal treatment on GO.

The XRD patterns of obtained RG nanosheets together with the precursor graphite and GO are displayed in Fig. 1(b). The XRD pattern of natural graphite reveals the characteristic intense diffraction peak of graphite at $2\theta = 26.4°$, which corresponds to the graphene interlayer of (002) with the d spacing of 0.34 nm [17,21,24,26]. The disappearance of the characteristic graphite peak at 26.4° and the formation of a broad peak at 9.7° (d = 0.92 nm) of dried GO indicates the intercalation of hydroxyl, carbonyl and epoxide groups in graphite interlayer during the chemical oxidation process [17,21,27]. Abundant amounts of those functional groups were removed from the surface of GO during the

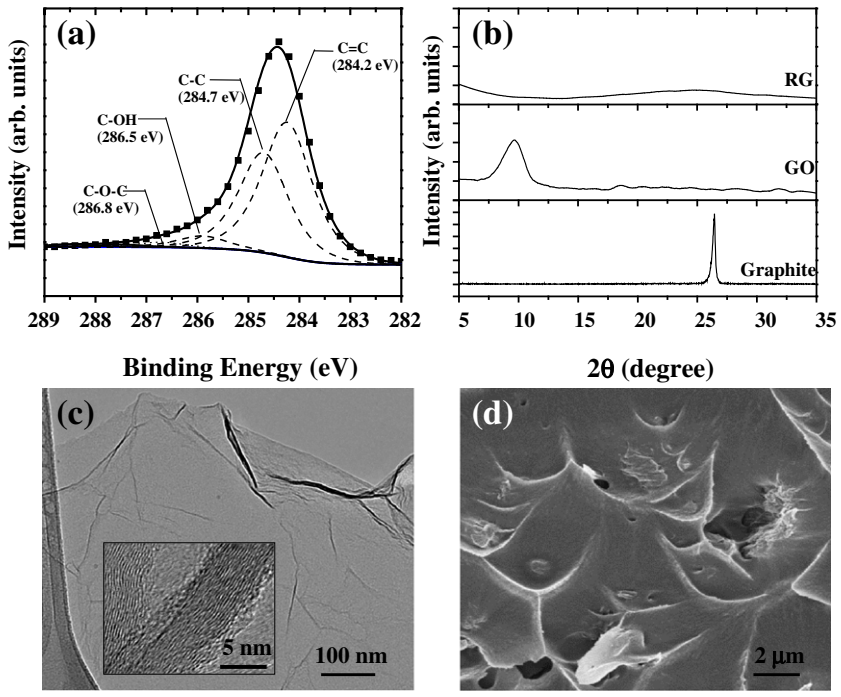

Fig. 1. (a) XPS spectra of RG. (b) XRD patterns of graphite, GO and RG. (c) TEM image of RG. *Inset*: High-magnified TEM image of RG edges. (d) SEM image of the fracture surface of PI/RG composite film.

thermal treatment to obtain RG as confirmed in the XPS results. The absence of significant diffraction peak in the XRD pattern of RG indicates the exfoliated feature of RG after the thermal reduction of GO.

Fig. 1(c) displays the of RG nanosheets on lacey carbon-coated copper grid. The ultra thin sheets with wrinkled, folded and silk-like morphology were observed in this TEM image together with the layered lattice structure of carbons in the edge or folding of RG from observed from high-magnified TEM image. The dispersion of RG in PI matrix is shown in Fig. 1(d). The interaction between PI and RG is strong that the detachment of RG from PI was not significant in the SEM image. In addition, the plastic deformation of PI matrix observed from the fracture surface indicates the enhanced mechanical strength by RG.

3.2. Characteristics of deposited thin film on PI

The barrier thin film was deposited on the transparent PI/RG or PI/GO films using an RF magnetron sputtering system with a Si_3N_4 target and under Ar. No diffraction peaks on XRD patterns were observed on the deposited thin film on each PI nanocomposite indicating the amorphous structure of each deposited thin film. XPS depth-profiling was conducted to investigate the chemical binding state of films. The full-survey XPS spectra of the deposited thin films confirm the presence of Si, O, N, and C elements on each specimen. Fig. 2 shows the atomic composition of the 100 nm-thick deposited film on pure PI film as a function of sputtering time. Before sputtering, the relative composition of each element in thin film was 22.1% (Si), 2.1% (N), 48.6% (O) and 27.2% (C). The atomic ratio of O to Si is 2.2 and the ratio of N to Si is 0.095, which is much lower than that of Si_3N_4 stoichiometry. Fig. 3(a) displays the deconvolution results of Si2p XPS spectra at the topmost surface and confirms the presence of SiO_2, SiN_xO_y and SiN_x [28,29]. The oxidation process may continue on the topmost surface of deposited thin film [30] that the atomic ratio of O to Si was as high as 2.2. The deconvoluted N1s XPS peaks shown in Fig. 3(c) display the Si–N and Si–N–O binding states [19], which are in agreement with the Si2p results. Moreover, the deconvolution of O1s XPS spectrum (Fig. 3(e)) confirms the dominant Si–O–Si and Si–O–N peaks [29,31] on the surface of barrier layer.

The atomic composition of deposited layer is uniform within the 100 nm thickness as shown in Fig. 2. After removal of the topmost surface layer, the carbon content dramatically dropped to 2.9% and the atomic composition of Si, O, and N is 30.3%, 64.5%, and 2.2%, respectively. The relative composition of O to Si within the deposited barrier layer is still around 2.1. And the ratio of N to Si is 0.073, which is lower than the stoichiometric N/Si ratio of Si_3N_4. Fig. 3(b, d) shows the deconvolution results of Si2p and N1s photoelectrons from the PI film after 2-min Ar^+ sputtering (i.e. about the depth of 30 nm below the surface). The Si2p deconvoluted peaks demonstrate the signals with the binding energy of SiO_2 at 103.5 eV [28,29] as well as that of SiN_xO_y at 102.2 eV, which is the intermediate state between silicon oxynitride and silica [29,32]. The deconvolution result of N1s photoelectrons shown in Fig. 3(d) displays the Si–N and Si–N–H binding states similar to Fig. 3(c). No characteristic Si_3N_4 peak at 397.4 eV [33] is shown from the deconvoluted XPS results. A lower binding energy of 396.1 eV is assigned to the N–O chemical state in the deposited barrier layer. The high oxygen content in the

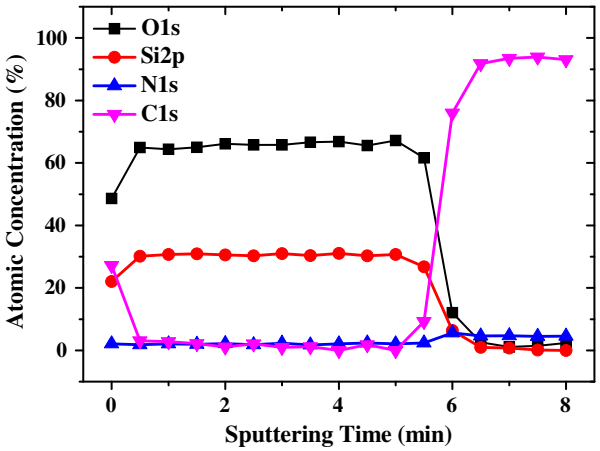

Fig. 2. The XPS depth profile results of the deposited barrier layer (thickness = 100 nm) on PI film. Note: the sputtering rate is 14.3 nm/min.

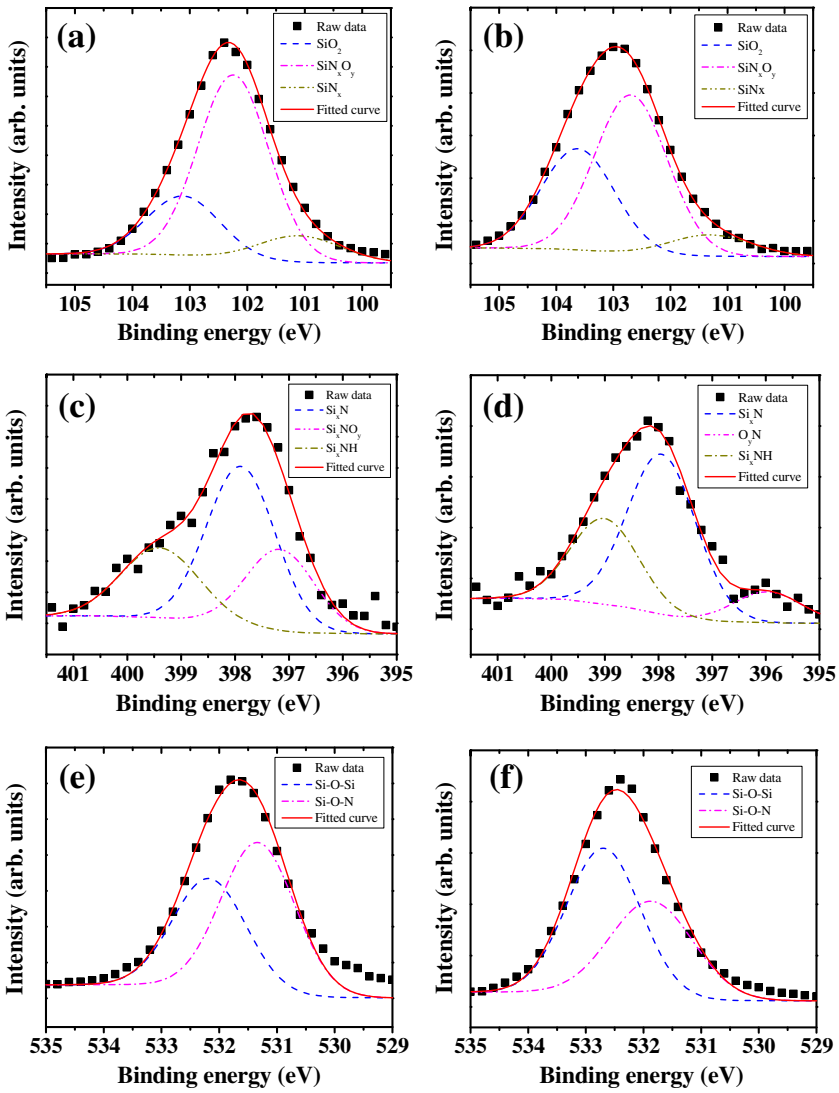

Fig. 3. Deconvolution results of XPS spectra in (a, b) Si2p, (c, d) N1s, and (e, f) O1s regions of the barrier layer (thickness = 100 nm) deposited on PI film. (a, c, e) The results from the surface of barrier layer (i.e. before Ar^+-sputtering). (b, d, f) The results from the middle of barrier layer (i.e. Ar^+-sputtering time = 2 min).

barrier layer is due to the high affinity of silicon to oxygen. Very trace amount of water or oxygen-containing impurity in the sputtering chamber will induce the formation of silicon oxide [28,29,31]. The Si – O and Si – O – N states at 532.8 and 531.6 eV, respectively, are deconvoluted from the barrier layer as shown in Fig. 3(f). Besides, the carbon within barrier layer comes from the trace amount of organic impurity in sputtering chamber. The increase in carbon ratio was observed in Fig. 2 when the depth profiling time is longer than 360 s, i.e. reaching the interface of barrier layer and the organic polyimide film. The high composition of carbon comes from the organic structure of PI film. A reactive sputtering condition, such as using H_2/Ar gas mixture [28], or increasing the substrate temperature [33], is suggested to ensure the formation of stoichiometric silicon nitride.

The morphology of the deposited layer on the transparent PI film was investigated by SEM images. The differences in the morphology between the barrier layer on pure PI or PI nanocomposite films are negligible. A similar average grain size of barrier layer particles is observed previously on different PI matrices [14] using identical RF sputtering system. However, as shown in a series of SEM images, the morphology of barrier layer is significantly affected by the sputtering conditions, especially the working pressure. Fig. 4 shows the SEM images of barrier layer deposited on pure PI under the same working pressure (4 mTorr) and various sputtering powers (50, 80, and 100 W). When the sputtering power is 50 W, the atoms ejected from the target have insufficient energy to allow the surface diffusion or clustering on the surface of PI film. Hence, a smaller grain size of the particles was observed from the deposition layer (Fig. 4(a)). In contrast, the ejected atoms possessed sufficient energy to diffuse on the substrate and to cluster with other atoms when the sputtering power is as high as 100 W. The migration and aggregation of atoms are so fast that the surface of deposited layer was relatively heterogeneous as shown in Fig. 4(c). The sputtering power of 80 W is the best condition to balance the rates of diffusion and clustering of atoms on the PI substrates that a uniform barrier layer is obtained as shown in Fig. 4(b). The deposition thickness of barrier layers shown in Fig. 4(a–c) is 30 nm, which is the optimum deposition thickness to obtain continuous thin films without the formation of cracks. Surface cracks were observed from the thicker barrier films (thickness > 50 nm) because of the accumulated internal stress in the barrier layer [9]. Fig. 4(d) illustrates the cracks on the barrier thin films with the thickness of 50 nm using the sputtering conditions identical to Fig. 4(b). At the same sputtering power of 80 W, the increasing working pressure from 4 to 8 mTorr leads to the increasing of mean free path of ejected atoms from the target; consequently, those atoms that arrive on the PI substrate will have lower energy that the barrier layer is loosely packed or crakes are easily produced.

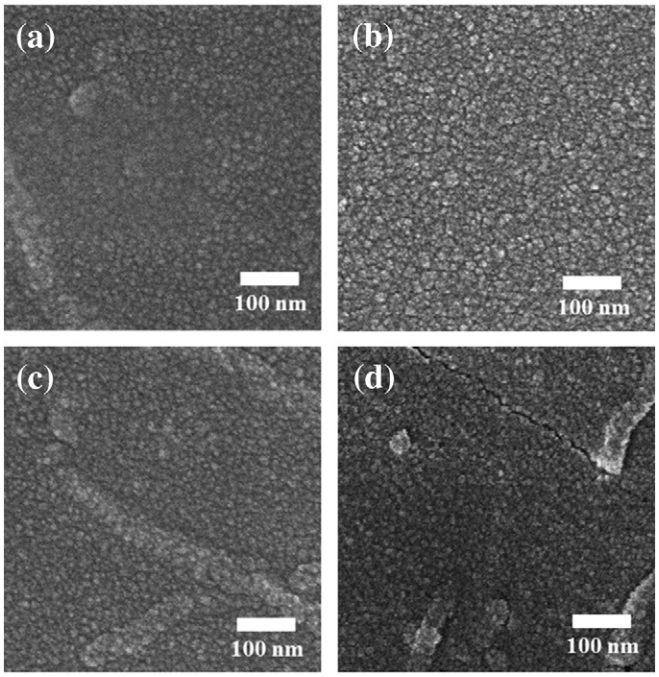

Fig. 4. SEM images of the surface of deposited barrier thin films (thickness = 30 nm) on PI films under the working pressure of 4 mTorr and the sputtering power of (a) 50 W, (b) 80 W, and (c) 100 W. (d) SEM image of the surface of deposited barrier thin film with the thickness of 50 nm under working pressure of 4 mTorr and the sputtering power of 80 W.

Those differences in the morphology of deposited thin films significantly affect the water barrier properties of each deposited PI or PI nanocomposite films.

3.3. Water barrier properties of deposited PI, PI/RG and PI/GO films

The water barrier property of each film was determined by using the commercial MOCON instrument. The WVTR of pure PI film with the thickness of 25 μm (i.e. 1 mil) is as high as 181 g/m^2-day. The barrier layer was deposited on pure PI to improve its water barrier property. As discussed in the previous section, the sputtering conditions affect the morphology of barrier layer, and thus influence the water barrier properties of films. Fig. 5 illustrates the WVTR of pure PI films deposited with barrier layers with various thicknesses under different sputtering conditions. At the working pressure of 4 mTorr, the deposited thin film shows a better water barrier property than those using a higher working pressure. The lowest WVTR ranging from 1 to 3 g/m^2-day is obtained from the PI film deposited with a 30 nm-thick barrier layer regardless of the sputtering conditions. As confirmed by the SEM images, the close-packing of particles on PI effectively reduce the water diffusion rate through the barrier layer.

Fig. 6 shows the WVTR values of as-prepared pure PI and PI nanocomposite films containing GO or RG not higher than 0.1 wt.%. Before barrier layer deposition, a dramatic decrease in WVTR by 92.8%, i.e. 13 g/m^2-day, is achieved upon the addition of only 0.1 wt.% of RG in transparent PI matrix. The WVTR of PI/GO-0.1 is 32 g/m^2-day. A continuous decrease in WVTR with the increasing RG or GO content was observed. However, the optical transparency of PI/RG with the RG content higher than 0.3 wt.% is less than 80% in the visible light region. The decrease in WVTR by GO is not as remarkable as RG because the moisture absorption capacity of PI/RG is found lower than that of PI/GO and pure PI. Graphene nanosheets have been considered being impermeable to gases and can support pressure differences larger than 1 atm [34]. Furthermore, the distribution of those nanosheets with the features of high aspect ratio and high specific surface area in PI matrix can effectively extend the path of the water vapor passing through the thin film [15,16,20]

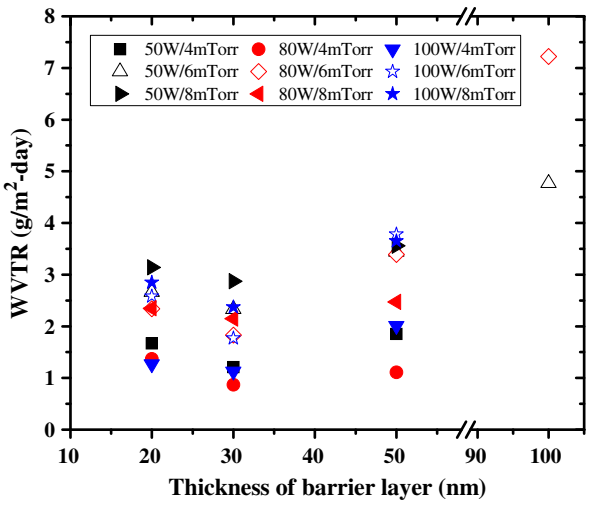

Fig. 5. Effects of the thickness of barrier layer and the sputtering parameters on the WVTR of pure PI. The WVTR of pure PI before sputtering is 181 g/m^2-day.

and thus significantly improve water vapor barrier property. At the same weight content of filler, the volume of RG was larger than that of GO because RG has smaller density than GO. Moreover, the surface of PI/RG-0.1 was more hydrophobic than that of PI/GO-0.1 [17]. Consequently, the water barrier property of RG is superior to that of GO in PI nanocomposite films with identical weight percentage of filler.

The optimum sputtering condition, i.e. the sputtering power of 80 W and the working pressure of 4 mTorr, obtained from pure PI also produce close-packed barrier layers on other PI nanocomposites. Fig. 6 plots the WVTR of PI and PI nanocomposites as a function of the thickness of the barrier layer sputtered using the above condition. The WVTR of each film decreases with the barrier layer thickness up to 30 nm. An increase in WVTR was observed for films deposited with a barrier layer thicker than 30 nm because of the formation of cracks on the thick barrier film as evidenced in the SEM images. Recall that, the WVTR of pure PI is 181 g/m^2 day. After deposited with a 30-nm thick barrier layer on pure PI, the WVTR of 30Si-PI is 0.9 g/m^{2}day, which is only 0.5% of as-prepared pure PI. Under the same deposition condition, the WVTR of Si-30/PI/RG-0.1 further decreases to 0.17 g/m^{2}day, which is 1.3% of un-deposited PI/RG-0.1. The reduction in the WVTR of PI by 0.1 wt.%

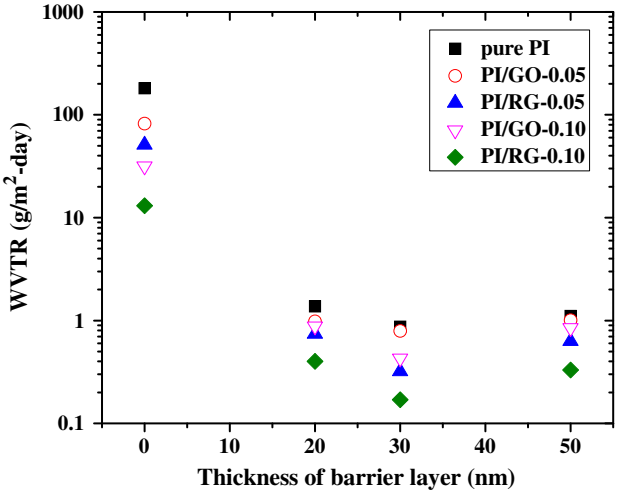

Fig. 6. Effects of filler content and thickness of barrier layer on the WVTR of pure PI, PI/GO and PI/RG nanocomposite films. The barrier layer was deposited under the working pressure of 4 mTorr and the sputtering power of 80 W.

of RG is 92.8% and by 30 nm-thick-barrier-layer is 99.5%, respectively. The WVTRs of PI films deposited with a 30-nm thick barrier layer are lower than 1 g/m^2-day. Notably, those PI films deposited with a barrier layer show excellent optical, thermal and thermal properties.

3.4. Optical, thermal and mechanical properties of PI nanocomposites

The UV–vis spectra of pure PI and PI/RG-0.1 before barrier layer deposition are shown in the *inset* in Fig. 7. The transparency of PI/RG-0.1 is lower than that of pure PI. Moreover, the optical transmittance of PI/GO-0.1 is higher than that of PI/RG-0.1 due to the better dispersion of GO than that of RG in PI matrix. The overlapping of RG nanosheets in PI matrix results in the reduction in the optical transmittance; however, it improves the water barrier property of PI film. The transmission at the wavelength of 550 nm is chosen as an indicator of the optical transparency of each film and plotted as a function of barrier layer thickness in Fig. 7. The optical transparency remains at least 80% when the PI films are deposited with a barrier layer less than 50 nm. Notably, the surface roughness of deposited barrier layer on PI is less than 5 nm as confirmed by AFM indicating its potential application as a transparent substrate in flexible electronics.

Table 1 summarizes the properties of pure PI and PI nanocomposite films with the thickness of 25 μm. The storage modulus (E′) of PI nanocomposite films increase remarkably with the increasing RG content. The E′ value at 60 °C is 1487 MPa for pure PI and increases to 2278 MPa for PI/RG-0.1. The glass transition temperature (Tg) of PI films is determined from the peak of tan delta curve of each sample. The Tg values of PI and PI/RG are around 349 °C suggesting their sufficient thermal stability for industry application. The simple solution-blending process of RG with PI did not change the imidization degree or the chain configuration of PI. For pure PI, the modulus at initial 2% elongation is as high as 1 GPa and the elongation at break is more than 100%. The PI films containing 0.1 wt.% RG or GO exhibit similar strength. In addition, the tensile strength of PI/RG was slightly higher than that of pure PI indicating the non-covalent interaction between PI and RG phases [35]. The thermal decomposition temperature (Td_5) at 5% weight loss is 431 °C for PI/RG-0.1 compared to 427 °C for pure PI. The thermal stability of PI is enhanced by the blending of thermally stable RG in PI solution. The incorporation of tiny amount of RG significantly drops the CTE to 48 ppm/°C for PI/RG-0.1 compared to 59 ppm/°C for pure PI. The reduction in CTE by almost a factor of 20% at 0.1 wt.% RG loading is significant. The addition of those nearly one-dimensional RG nanosheets is believed to enhance the chain orientation of PI and thus a lower CTE was observed [36].

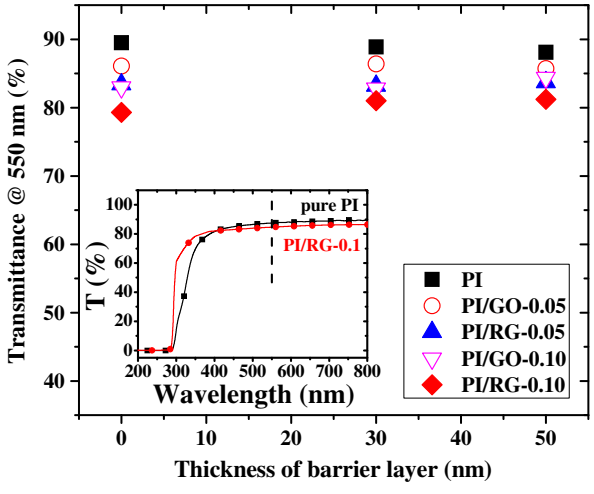

Fig. 7. Effect of barrier layer thickness on the optical transmittance (at 550 nm) of various PI films. *Inset*: UV–vis spectra of as-prepared PI and PI/RG-0.1.

Table 1
Properties of pure PI, PI/GO and PI/RG films before barrier layer deposition.

Sample	DMA				TMA	TGA	WVTR[g] (g/m^2-day)
	E′[a] (MPa)	Tg[b] (°C)	E[c] (GPa)	TS[d] (MPa)	CTE[e] (ppm/°C)	Td_5[f] (°C)	
Pure PI	1487	349	1.1	85	59	427	181
PI/RG-0.1	2278	346	1.1	95	48	431	13
PI/GO-0.1	1637	347	1.1	90	41	422	32

[a] Storage modulus at 60 °C.
[b] The temperature at the maximum of Tan δ curve was designated as Tg.
[c] Modulus at 2% elongation.
[d] Tensile strength.
[e] The coefficient of thermal expansion (CTE) determined over the range of 100–200 °C.
[f] The thermal decomposition temperature at 5% weight loss.
[g] Water vapor transmission rate (WVTR) measured at 40 °C and 100% RH.

4. Conclusions

Combining solution-blending nanofillers RG or GO in transparent PI matrix and depositing a single layer of barrier film on the surface of PI efficiently enhanced the moisture resistance of transparent PI films. The WVTR decreases from 181 g/m^2-day of the transparent PI to 13 g/m^2-day of PI containing 0.1 wt.% of RG. The close-packed and continuous barrier film on PI/RG-0.1 together with the improved hydrophobicity of PI/RG further reduce the WVTR to 0.17 g/m^2-day by a factor of 99.5%. The optimum deposition thickness of the moisture barrier film for the minimizing the WVTR is 30 nm regardless of the types of PI substrates or the sputtering conditions. The flexible Si-30/PI/RG-0.1 film remains with high optical clarity and simultaneously shows excellent water barrier performance, enhanced dimensional stability and sufficient mechanical strength for advanced electronic applications.

Acknowledgments

The authors would like to acknowledge the financial support from the Ministry of Economic Affairs, Taiwan, through the project on flexible polymeric materials for electronic application (100-EC-17-A-07-S1-120). We also acknowledge the support from the National Science Council of Taiwan under the grant number of NSC 100-2221-E-167-006.

References

[1] K. Fukukawa, M. Okazaki, Y. Sakata, T. Urakami, W. Yamashita, S. Tamai, J. Photopolym. Sci. Technol. 24 (3) (2011) 255.
[2] J.H. Park, J.H. Kim, J.W. Park, J.H. Chang, C.S. Ha, J. Nanosci. Nanotechnol. 8 (4) (2008) 1700.
[3] M.C. Choi, Y. Kim, C.S. Ha, Prog. Polym. Sci. 33 (6) (2008) 581.
[4] M.C. Choi, J.C. Hwang, C. Kim, S. Ando, C.S. Ha, J. Polym. Sci. Polym. Chem. 48 (8) (2010) 1806.
[5] P.F. Carcia, R.S. McLean, M.D. Groner, A.A. Dameron, S.M. George, J. Appl. Phys. 106 (2) (2009).
[6] H. Zervos, Barrier Films for Flexible Electronics, IDTechEx, 2009.
[7] S.H. Park, H.S. Lee, J.H. Choi, C.M. Jeong, M.H. Sung, H.J. Park, J. Appl. Polym. Sci. 125 (2012) E675.
[8] S.J. Patil, D.S. Bodas, G.J. Phatak, S.A. Gangal, Bull. Mater. Sci. 25 (5) (2002) 399.
[9] D.S. Wuu, T.N. Chen, E. Lay, C.H. Liu, C.H. Chang, H.F. Wei, L.Y. Jiang, H.U. Lee, Y.Y. Chang, J. Electrochem. Soc. 157 (2) (2010) C47.
[10] J.W. Han, H.J. Kang, J.H. Kim, D.S. Seo, Y.H. Kim, D.G. Moon, J.I. Han, Mol. Cryst. Liq. Cryst. 458 (2006) 255.
[11] J.J. Burack, J.D. LeGrange, A.W. Lin, IEEE Trans. Components Hybrids Manuf. Technol. 13 (1990) 214.
[12] G.F. Sykes, A.K. St. Clair, J. Appl. Polym. Sci. 32 (1986) 3725.
[13] M.H. Tsai, H.Y. Wang, H.T. Lu, I.H. Tseng, H.H. Lu, S.L. Huang, J.M. Yeh, Thin Solid Films 519 (15) (2011) 4969.
[14] I.H. Tseng, C.J. Chang, C.W. Chang, H.H. Lu, M.H. Tsai, Surf. Coat. Technol. (2012), http://dx.doi.org/10.1016/j.surfcoat.2012.07.038.
[15] O.C. Compton, S. Kim, C. Pierre, J.M. Torkelson, S.T. Nguyen, Adv. Mater. 22 (42) (2010) 4759.
[16] H. Kim, Y. Miura, C.W. Macosko, Chem. Mater. 22 (11) (2010) 3441.
[17] I.H. Tseng, Y.F. Liao, J.C. Chiang, M.H. Tsai, Mater. Chem. Phys. 136 (1) (2012) 247.
[18] M.A. Signore, A. Sytchkova, D. Dimaio, A. Cappello, A. Rizzo, Opt. Mater. 34 (4) (2012) 632.
[19] Y.S. Hirohata, N. Hino, T. Yamashima, K. Yabe, Thin Solid Films 253 (1-2) (1994) 425.

[20] H.M. Kim, J.K. Lee, H.S. Lee, Thin Solid Films 519 (22) (2011) 7766.
[21] N.D. Luong, N. Pahimanolis, U. Hippi, J.T. Korhonen, J. Ruokolainen, L.S. Johansson, J.D. Nam, J. Seppala, J. Mater. Chem. 21 (36) (2011) 13991.
[22] J.Y. Wang, S.Y. Yang, Y.L. Huang, H.W. Tien, W.K. Chin, C.C.M. Ma, J. Mater. Chem. 21 (35) (2011) 13569.
[23] D. Yang, A. Velamakanni, G. Bozoklu, S. Park, M. Stoller, R.D. Piner, S. Stankovich, I. Jung, D.A. Field, C.A. Ventrice Jr., Carbon 47 (1) (2009) 145.
[24] I.H. Tseng, J.C. Chiang, S.L. Huang, M.H. Tsai, Polym. Int. (2011), http://dx.doi.org/10.1002/pi.4375.
[25] C.C. Teng, C.C.M. Ma, C.H. Lu, S.Y. Yang, S.H. Lee, M.C. Hsiao, M.Y. Yen, K.C. Chiou, T.M. Lee, Carbon 49 (15) (2011) 5107.
[26] G.X. Wang, J. Yang, J. Park, X.L. Gou, B. Wang, H. Liu, J. Yao, J. Phys. Chem. C 112 (22) (2008) 8192.
[27] D. Chen, H. Zhu, T. Liu, ACS Appl. Mater. Interfaces 2 (12) (2010) 3702.
[28] A.F.A. Batan, J. Vereecken, F. Reniers, Surf. Interface Anal. 40 (2008) 754.
[29] S.M. Castanho, R. Moreno, J.L.G. Fierro, J. Mater. Sci. 32 (1) (1997) 157.
[30] J. Szepvolgyi, I. Mohai, J. Gubicza, J. Mater. Chem. 11 (3) (2001) 859.
[31] R. Hofman, J.G.F. Westheim, I. Pouwel, T. Fransen, P.J. Gellings, Surf. Interface Anal. 24 (1) (1996) 1.
[32] F. Henry, C.Y. Duluard, A. Batan, F. Reniers, Thin Solid Films 520 (20) (2012) 6386.
[33] M.C. Poon, C.W. Kok, H. Wong, P.J. Chan, Thin Solid Films 462 (2004) 42.
[34] J.S. Bunch, S.S. Verbridge, J.S. Alden, A.M. van der Zande, J.M. Parpia, H.G. Craighead, P.L. McEuen, Nano Lett. 8 (8) (2008) 2458.
[35] G.Y. Kim, M.C. Choi, D. Lee, C.S. Ha, Macromol. Mater. Eng. 297 (4) (2012) 303.
[36] S. Ebisawa, J. Ishii, M. Sato, L. Vladimirov, M. Hasegawa, Eur. Polym. J. 46 (2) (2010) 283.